Monitoring and numerical modelling of riverbank erosion processes: a case study along the Cecina River (Central Italy).

EARTH SURFACE PROCESSES AND LANDFORMS
Earth Surf. Process. Landforms **34**, 530–546 (2009)

Published online 1 December 2008 in Wiley InterScience
(www.interscience.wiley.com) DOI: 10.1002/esp.1754

Monitoring and numerical modelling of riverbank erosion processes: a case study along the Cecina River (central Italy)

Laura Luppi,[1] Massimo Rinaldi,[1]* Liliana B. Teruggi,[1] Stephen E. Darby[2] and Laura Nardi[1]
[1] Department of Civil and Environmental Engineering, University of Florence, Via S. Marta 3, Firenze 50139, Italy
[2] School of Geography, University of Southampton, Highfield, Southampton SO17 1BJ, UK

Received 21 April 2008; Revised 5 August 2008; Accepted 15 August 2008

* Correspondence to: Massimo Rinaldi, Department of Civil and Environmental Engineering, University of Florence, via S. Marta 3, 50139 Firenze, Italy.
E-mail: mrinaldi@dicea.unifi.it

ESPL
Earth Surface Processes and Landforms

ABSTRACT: Riverbank retreat along a bend of the Cecina River, Tuscany (central Italy) was monitored across a near annual cycle (autumn 2003 to summer 2004) with the aim of better understanding the factors influencing bank changes and processes at a seasonal scale. Seven flow events occurred during the period of investigation, with the largest having an estimated return period of about 1·5 years. Bank simulations were performed by linking hydrodynamic, fluvial erosion, groundwater flow and bank stability models, for the seven flow events, which are representative of the typical range of hydrographs that normally occur during an annual cycle. The simulations allowed identification of (i) the time of onset and cessation of mass failure and fluvial erosion episodes, (ii) the contributions to total bank retreat made by specific fluvial erosion and mass-wasting processes, and (iii) the causes of retreat. The results show that the occurrence of bank erosion processes (fluvial erosion, slide failure, cantilever failure) and their relative dominance differ significantly for each event, depending on seasonal hydrological conditions and initial bank geometry. Due to the specific planimetric configuration of the study bend, which steers the core of high velocity fluid away from the bank at higher flow discharges, fluvial erosion tends to occur during particular phases of the hydrograph. As a result fluvial erosion is ineffective at higher peak discharges, and depends more on the duration of more moderate discharges. Slide failures appear to be closely related to the magnitude of peak river stages, typically occurring in close proximity to the peak phase (preferentially during the falling limb, but in some cases even before the peak), while cantilever failures more typically occur in the late phase of the flow hydrograph, when they may be induced by the cumulative effects of any fluvial erosion.

KEYWORDS: riverbank erosion; riverbank retreat; fluvial erosion; mass failures; Cecina River, Italy

Introduction

Bank retreat is the integrated product of three interacting processes (i.e. weathering and weakening, fluvial erosion and mass-wasting), with mass failures and fluvial erosion typically dominating in the middle to lower portions of a drainage basin (Lawler, 1992). In recent years the role of subaerial processes (weathering and weakening) as a mechanism for enhancing bank erodibility and promoting fluvial erosion has started to be recognized (e.g. Lawler, 1993; Prosser *et al.*, 2000; Couper and Maddock, 2001), although their quantification is extremely complex. Similarly, progress has been made in understanding and quantifying mass failures, with a wide range of studies elucidating the role of bank hydrology (e.g. Casagli *et al.*, 1999; Rinaldi and Casagli, 1999; Simon *et al.*, 2000; Dapporto *et al.*, 2001, 2003; Rinaldi *et al.*, 2004), and riparian vegetation (e.g. Abernethy and Rutherfurd, 1998, 2000; Simon and Collison, 2002; Pollen and Simon, 2005; Pollen, 2006; Van de Wiel and Darby, 2007; Pollen-Bankhead and Simon, 2008). Progress has also been made in understanding and quantifying other processes, such as seepage erosion and its contribution to mass failures (Fox *et al.*, 2006, 2007; Wilson *et al.*, 2007).

In contrast, although improvements in the modelling of near-bank flows are starting to be made (e.g. Kean and Smith, 2006a,b), there are still relatively few studies (e.g. Julian and Torres, 2006; Papanicolau *et al.*, 2007) that have quantified the process of fluvial erosion (i.e. the removal of bank sediments by the direct action of the flow). Observed rates of fluvial erosion range over several orders of magnitude (Hooke, 1980), and poor correlations have been found between measured rates of bank retreat and bulk flow parameters describing the magnitude (i.e. peak discharge) of erosive events, due to the inherent extreme variability of the relevant controlling parameters. Likewise, with a few notable exceptions (Simon *et al.*, 2003, 2006; Darby *et al.*, 2007), few studies have been concerned with elucidating the interaction between fluvial erosion and mass failure, and this represents an important limitation because dynamic interactions and feedbacks between processes may lead to outcomes that are not predictable a

priori (Rinaldi and Darby, 2008). This is in part explainable by the extreme difficulties associated with measuring bank changes and discriminating the contribution of different processes at the scale of a single flow event. In fact, logistical and safety concerns usually limit the frequency of monitoring to relatively coarse timescales, at best perhaps resolving individual flow events, while it is clear that greater (subevent scale) temporal resolution is needed to resolve key aspects such as onset and cessation thresholds, rates and process dynamics (Lawler, 2005a,b; Rinaldi and Darby, 2008). An alternative way forward, therefore, is to use numerical simulations, parameterized with high quality field data, to reproduce and quantify the different processes and their interactions. This would provide a means to achieve a realistic quantification of the processes at the intra-event timescale, in turn allowing for a better understanding of issues such as the time of onset and cessation of the different processes, their interaction, and their respective contributions to the total volumes of eroded bank sediment.

This study starts with a monitoring activity carried out over a seasonal cycle (autumn 2003 to summer 2004) on an eroding outer bank located along a channel bend of the Cecina River in Tuscany, central Italy. We then seek to develop insights into the dynamics of bank erosion at this site using a modelling approach that builds on recent work by Darby *et al*. (2007), in which fluvial erosion, groundwater flow and stability analyses are fully integrated. A further development of the Darby *et al*. (2007) model is adopted in this study, by adding a hydrodynamic component to evaluate near-bank shear stresses more accurately. For a detailed description of the methodology and the model parameterization for the Cecina riverbank, we refer to the paper of Rinaldi *et al*. (2008a). In contrast, this paper focuses on extending the discussion of the results to include the full range (seven) of flow events that occurred in the monitoring period. This enables us to explore the influence on bank erosion of different hydrograph characteristics and initial conditions, representative of the range of hydrological events encountered in a seasonal cycle.

The objectives of this paper therefore can be summarized as follows: (1) to describe and discuss the monitoring results from a case study of bank retreat with a complex channel geometry; (2) to quantify, via numerical simulation, the different processes (fluvial erosion and mass failure) and their mutual role at the intra-event timescale, for a variety of flow events during a seasonal cycle.

Study Area

The Cecina River is located in central Tuscany (Italy) (Figure 1A). The catchment has an area of about 905 km^2, and the river has a total length of about 79 km, outflowing into the Tyrrhenian Sea roughly 50 km south of Pisa. The middle and lower portion of the catchment is dominated by hilly slopes composed of erodible fluvio-lacustrine and marine sediments (Upper Miocene, Plio-Pleistocene), with relatively low relief. The area falls

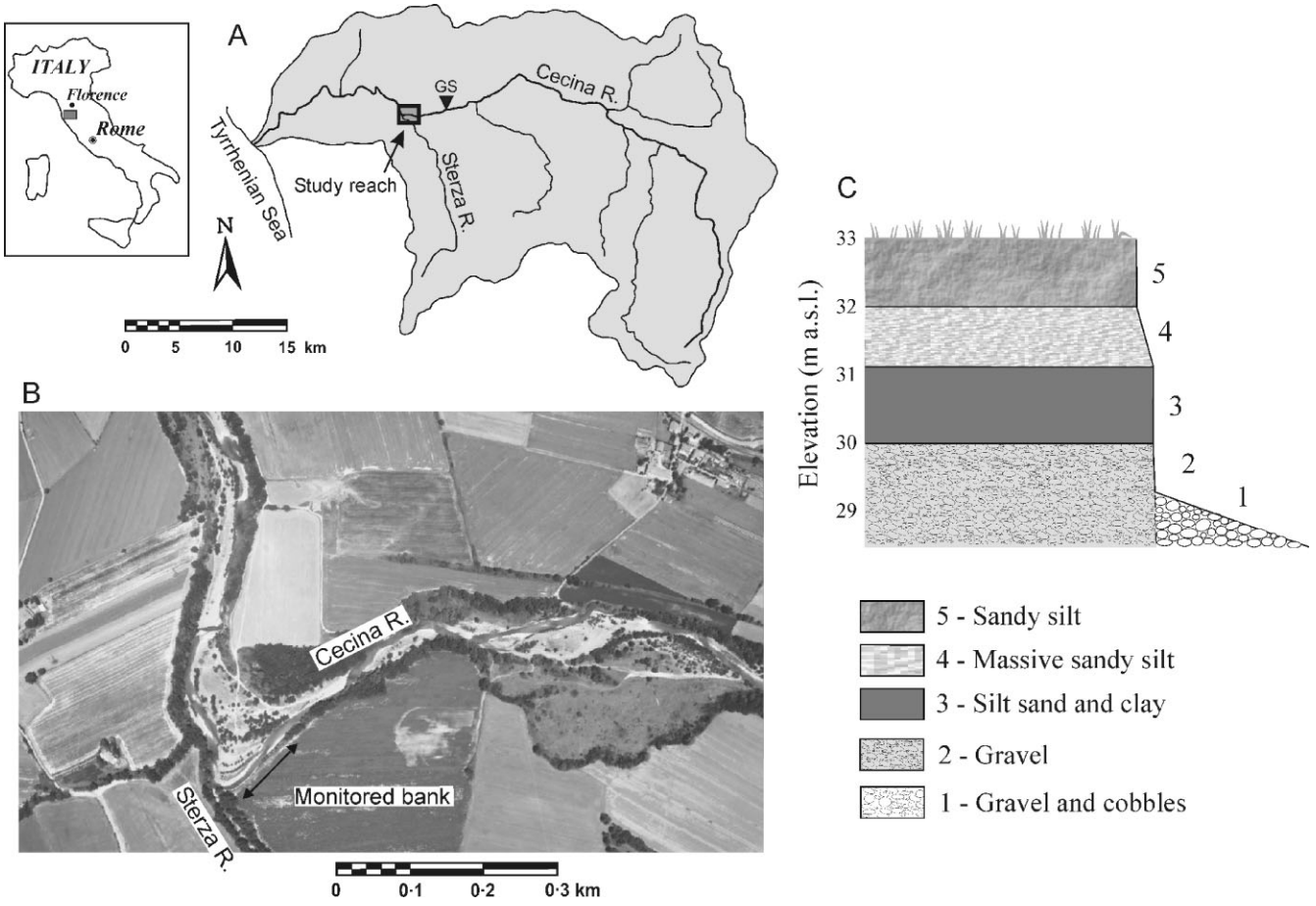

Figure 1. Study area. (A) Cecina basin and location of the study reach (GS: gauging station). (B) 2004 aerial photograph (1:10 000 scale) showing the study reach and monitored bank (aerial photograph reproduced by permission of Provincia di Pisa). (C) River bank stratigraphy: 1, loose gravel and cobbles; 2, gravel (D_{50} = 13 mm; thickness ranging from 185 to 225 cm); 3, silt, sand and clay (heterogeneous layer composed of alternating lenses of sand with D_{50} = 0·2 mm, sandy silt levels with D_{50} = 0·01 mm, and clayey silt horizons; total thickness ranging from 80 to 120 cm); 4, massive sandy silt (D_{50} = 0·05 mm; thickness ranging from 85 to 165 cm); 5, sandy silt (D_{50} = 0·05 mm, thickness ranging from 110 to 155 cm).

DOI: 10.1002/esp

within a temperate climatic zone with a dry season, i.e. the Mediterranean climate category, characterized by a high variability in flow discharges. The mean annual precipitation is about 944 mm.

The study reach (Figure 1B) is located along the middle–lower portion of the basin, at the confluence of the Sterza River, 20 km from the outlet and 2 km downstream of the main flow gauging station for the catchment (Ponte di Monterufoli; drainage area 634 km^2) (Figure 1A). Mean daily discharge at this gauging station is 7·61 m^3 s^{-1}, while the peak discharge with a 2-year return period (Q_2) is 322 m^3 s^{-1}. Along the middle reaches of the catchment, where the study site is located, the Cecina is predominantly sinuous and locally meandering, with well developed point- and alternate bar features, actively eroding banks, and a gravel-bed with a median particle diameter (D_{50}) varying in the range between about 14 and 45 mm (Rinaldi *et al.*, 2008b). Significant channel adjustments (i.e. incision and narrowing) have occurred along this reach during recent decades, as a result of a combination of human disturbances (i.e. land-use changes and sediment mining) (Rinaldi, 2003; Rinaldi *et al.*, 2008b).

Study site and riverbank properties

The study site is about 500 m long, including an actively eroding (left) bank of about 70 m in length. The average gradient of the reach here is 0·0021, while the D_{50} of the bed sediments is about 22 mm on the point bar, and 37 mm on riffles. For the purposes of this study, it was necessary to select an eroding riverbank sufficiently representative of the sedimentary and geomorphological conditions observed along the same river and along similar rivers in the region, to ensure that the methods of analysis and results can reasonably be applied to other similar situations. Therefore, the riverbank was selected on the basis of the following criteria: (a) the bank was actively retreating through a combination of fluvial erosion and mass failures; (b) bank composition, dominant erosion processes and channel morphology were similar to those observed at other sites along the same river and similar rivers in the region; (c) additionally, the site was located sufficiently close to a gauging station so that it was possible to use stage readings at the gauging station to establish the time series and frequencies of discharges at the study site.

The eroding bank within the study reach has a height ranging from 5·0 to 5·5 m, and it is layered. A full description is provided by Rinaldi *et al.* (2008a), but the general bank material stratigraphy is arranged as shown in Figure 1C. Although the bank stratigraphy is quite variable and includes several sedimentary layers, the bank in question can be described as being composed of a cohesive upper portion (layers 3–5) overlying a gravel toe (layers 1–2), as is commonly the case in upland and piedmont zones in Europe and elsewhere (Rinaldi *et al.*, 2004; Darby *et al.*, 2007), but it is distinct from the fine-grained bank settings that are more usually associated with lowland environments and which have been the subject of related research (e.g. Simon *et al.*, 2000; Simon and Collison, 2002).

Analysis of a sequence of available aerial photographs (1954, 1986, 1993, 1999, 2004) has shown a progressive bank retreat and accretion of the opposite point bar, with a total outer bank retreat of about 70 m at the bend apex. Bank changes were particularly intense after 1986, being triggered by a major flow event that occurred in 1991 (Q_{peak} = 380 m^3 s^{-1}). The mean annual rate of retreat during the overall period between the start of the process (1991) and 2004 is 4·2 m yr^{-1}, with a slightly decreasing rate during the most recent years (about 2·7 m yr^{-1} between 1999 and 2004).

Monitoring Bank Retreat

Monitoring activity

Monitoring activities at the study site were undertaken to evaluate bank retreat associated with individual flow events and included (a) topographic surveys and measurements of bank retreat after each erosive event, combined with (b) hydrological monitoring of river stage and water table. Full details of these activities are given by Rinaldi *et al.* (2008a), so only a summary is provided here.

An initial topographic survey was performed during summer 2003 using a total station (Leika Geotronics 440) to accurately characterize the bed and bank topography of the entire study reach (Figure 2) for subsequent hydrodynamic modelling. A network of vertical pins parallel to the bank edge was also established, with a series of 27 control sections (Figure 2), for prompt baseline resurvey with perpendicular offsets (Lawler, 1993) immediately after each flow event. These vertical pins were supplemented with a network of horizontal erosion pins at six representative cross-sections. In each case a set of three erosion pins was inserted in the middle–lower portion of the bank, and the exposed portion of the pin was measured after each flow event. Periodic topographic resurvey after erosive events also included the measurement of the bank toe position along the eroding bank.

Hydrological monitoring of river stage and water table within the bank was undertaken during the entire period of investigation (October 2003 to May 2004), using a river stage sensor (RS), and two piezometers, P1 and P2, installed at the upstream limit of the eroding bank (Figure 2) at a distance of 5 m and 3 m from the bank edge, respectively. The piezometers were installed at depths (5·86 and 6·08 m) that ensured they were always lower than the water table. The instruments were connected to a data logger recording data every 15 minutes. River stages and corresponding discharges were obtained from the gauging station (Ponte di Monterufoli) located about 2 km upstream, where rainfall data were also collected (by the National Hydrological Survey). A correlation between river stages at the monitored bank and corresponding stages at the gauging station was obtained, enabling the known water discharges to be associated with the measured river stage at the monitored bank. Finally, a series of 11 crest gauges were installed along the monitored reach, to define the water level profile and gradients at the peak stage of erosive events, for the purposes of hydrodynamic modelling calibration and verification.

Monitoring results

River stages during the monitoring period are shown in Figure 3, with more detailed information regarding each flow event summarized in Table I. Seven erosive flow events can be defined, of which three events (1, 3, 4) consisted of a single peak hydrograph, whereas the remaining four exhibited more complex hydrograph shapes, with one or more secondary peaks. The maximum peak stage was attained during event 2, on 26 November 2003, when the discharge reached a value of 256·0 m^3 s^{-1}, which corresponds to an estimated return period of 1·5 years. The longest period of high discharge occurred during event 5 (18/02/2004–04/03/2004), which was characterized by prolonged precipitation and a total duration of about 10 days, with four distinct peak stages.

The monitoring period can be considered as quite typical of the Cecina's annual hydrological regime, with the monthly precipitation during the monitoring period very similar to the

DOI: 10.1002/esp

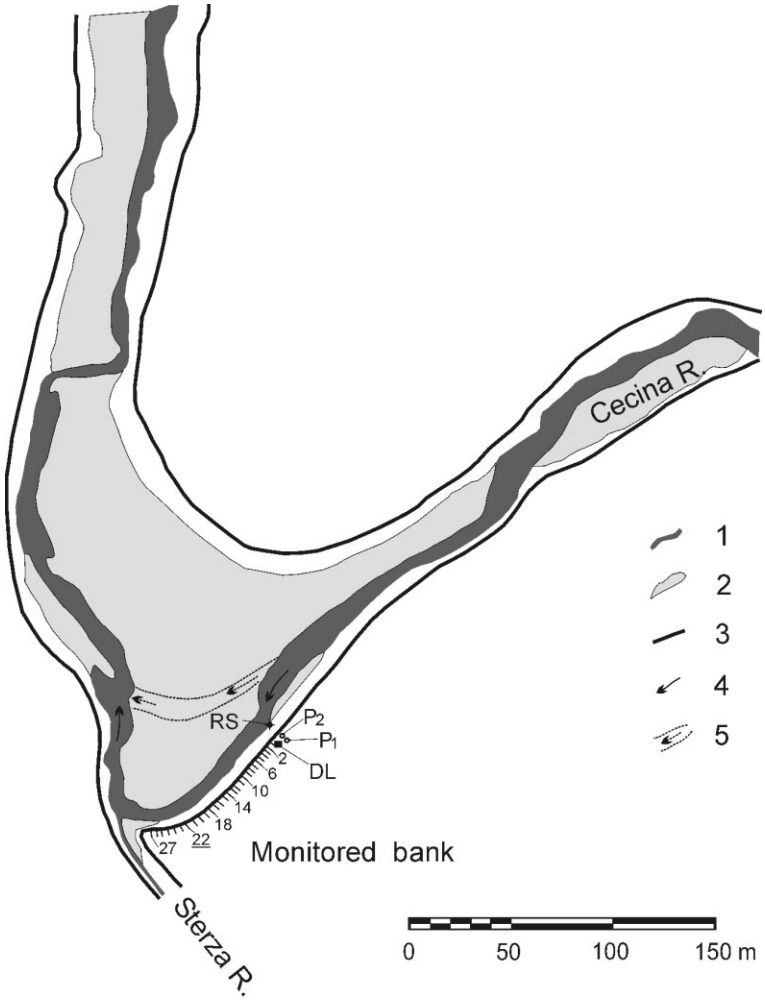

Figure 2. Study reach: channel morphology and monitoring setup. Main morphological features: 1, low-water channel; 2, bars; 3, bank edge; 4, flow direction; 5, chute channel with flow direction during high flows. Monitored bank: RS, river stage sensor; P1 and P2, piezometers; DL, datalogger numbers from 2 to 27 indicate control sections (22: bank section used for subsequent modelling).

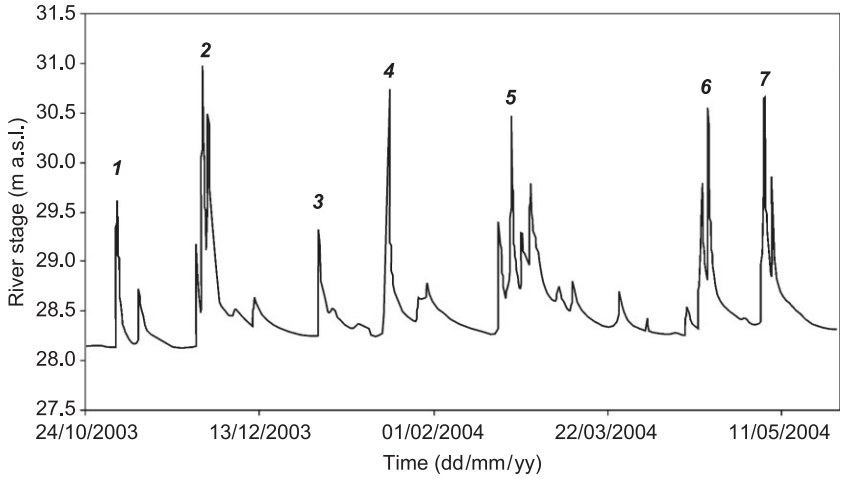

Figure 3. River stage during the period of investigation, indicating the seven main flow events (from 1 to 7) examined in this study (see details in Table I).

mean monthly precipitation based on data recorded over about 30 years. As is typical in this region, the highest flow events occurred during the Autumn months (in particular in November), with other significant flow events occurring in winter and spring. The number of events with a return period higher than 1 year observed during the monitoring period (5 events) is only slightly higher than the average value (4·3) calculated for the entire period of record (41 years) at the Ponte di Monterufoli gauge.

Regarding the spatial distribution of bank retreat observed during the entire monitoring period, a convenient way of visualizing this is to plot the progressive bank distance

DOI: 10.1002/esp

Table I. Summary of the main flow events observed during the monitoring period: *N*, progressive number of flow events; *H*, peak river stage (at the monitoring section); Q_{peak}, peak discharge; *T*, estimated return period (years)

N	Date	*H* (m a.s.l.)	Q_{peak} ($m^3 s^{-1}$)	*T* (years)
1	01/11/2003–04/11/2003	29·60	86·4	<1
2	24/11/2003–01/12/2003	30·96	256·0	1·5
3	29/12/2003–01/01/2004	29·32	59·6	<1
4	17/01/2004–28/01/2004	30·74	206·7	1·21
5	18/02/2004–04/03/2004	30·45	167·8	1·1
6	17/04/2004–05/05/2004	30·52	181·8	1·15
7	05/05/2004–28/05/2004	30·63	203·8	1·2

measured perpendicularly from the initial bank line (summer 2003) for the sequence of erosive events (Figure 4A). It has to be noted that it was not possible to distinguish the erosion caused by the events 6 (17/04/2004–05/05/2004) and 7 (05/05/2004–28/05/2004), because the second is a continuation of the first, preventing measurements being taken in the intervening period. Regarding the spatial pattern of bank retreat, it is possible to distinguish three main portions of the bank: (1) an upstream reach (the first 12 m) characterized by total bank retreat averaging 0·14 m; (2) a middle portion (from 12 to 45 m), delimited downstream by the point of maximum channel curvature, characterized by variable bank retreat with a mean of 1·96 m but a localized maximum reaching 3·5 m; (3) a downstream portion (from 45 to 70 m), characterized by more homogeneous and greater bank retreat, with a mean of 3·25 m and a local maximum of about 3·9 m. Regarding the temporal evolution of the bank deformation, it is evident that the first event (1–4 November 2003) induced significant bank retreat along most of the bank, although the peak discharge for this event (Q_{peak} = 86·4 $m^3 s^{-1}$) was relatively low. Event 2 (24 November to 1 December 2003; Q_{peak} = 256·0 $m^3 s^{-1}$) produced the most significant retreat, particularly along the downstream reach. Events 3 and 4 (29 December 2003 to 1 January 2004, Q_{peak} = 59·6 $m^3 s^{-1}$; and 11 January 2004 to 28 January 2004, Q_{peak} = 206·7 $m^3 s^{-1}$, respectively) produced a relatively low mean bank retreat, while more significant changes were again noted during the following three events (18 February 2004 to 4 March 2004, Q_{peak} = 167·8 $m^3 s^{-1}$; 17 April 2004 to 5 May 2004, Q_{peak} = 181·8 $m^3 s^{-1}$; 5 May 2004 to 28 May 2004, Q_{peak} = 203·8 $m^3 s^{-1}$).

To better analyse the magnitude of observed bank retreat in relation to the different flow events, Figure 4B plots the mean bank retreat for the middle and downstream portions of the bank (the upstream portion was excluded from this

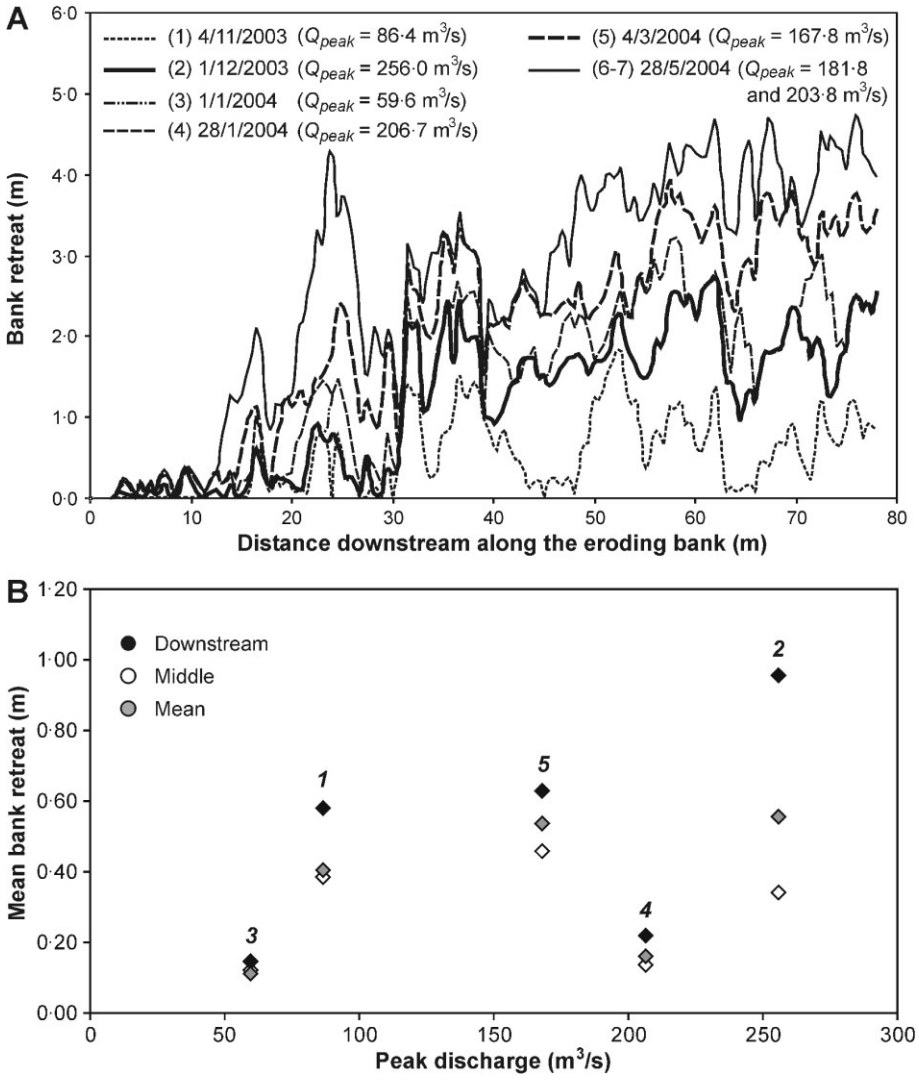

Figure 4. Bank retreat observed during the monitoring activity. (A) Bank retreat along the eroding bank for different surveys. The number of the erosive flow event is indicated in parentheses; the date indicates when the measurements were carried out. (B) Mean bank erosion for the middle and downstream portions of the study reach, and for the total length of the eroding bank (the upstream portion is not shown because of the limited retreat observed there) as a function of peak flow discharge (events 6 and 7 excluded for reasons described in the text).

DOI: 10.1002/esp

analysis because of the negligible changes there), and for the entire bank, versus the peak flow discharge. Flow events 6 and 7 are not included in the graph because it was not possible to discriminate the bank retreat of the two separate events for the reason explained before. It is evident that there is, at best, only a weak relationship between bank retreat and peak flow discharge. Although any trends in the data are weak, visual inspection of the graph suggests that the mean bank retreat for event 4 is particularly low, whereas for event 1 it is slightly higher than anticipated (particularly for the downstream portion of the bank). In fact, it is well known that relations between peak discharge and bank retreat are not well established (Hooke, 1980), suggesting that other factors play an important role in controlling the bank retreat. In this case it is probable that the excessive erosion of event 1 and the low erosion of event 4 are partly related to the initial conditions and to the characteristics of the flow, respectively. In fact event 1 was the first following the summer period, when the bank face was probably weakened by desiccation processes related to high temperatures (Prosser *et al*., 2000; Couper and Maddock, 2001), whereas event 4 was characterized by a very rapid ascending phase and a short total duration of the hydrograph. Further insights concerning the factors contributing to the different rates of bank retreat for the investigated flow events can be obtained from the modelling described in the following section, where the main processes and their controlling parameters are quantified, and therefore will be discussed later.

Bank Modelling

Full details of the modelling approach used here are available in Rinaldi *et al*. (2008a), which describes the complete model parameterization procedure for flow event 2. Here we merely summarize the methodology (Table II provides a summary of the parameter values used to represent the five sedimentary layers within the bank profile) prior to discussing the results. The modelling methodology is divided in two phases: (1) hydrodynamic modelling; (2) bank erosion modelling. In all cases simulations were undertaken for a representative bank profile located in the more active (downstream) portion of the eroding reach (profile 22 shown in Figure 2). This specific profile was selected because the observed retreat of this section (2·77 m) matches the mean rate of retreat measured along the actively eroding reach.

The hydrodynamic modelling was carried out using the software DELFT3D, developed by WL Delft Hydraulics and Delft University (WL Delft Hydraulics, 2006), employed here as a two-dimensional depth averaged hydrodynamic numerical model with a fixed, orthogonal-curvilinear, boundary fitted grid. The model used here, full details of the implementation of which are given by Mengoni (2004) and Mengoni and Mosselman (2005), solves the depth-averaged unsteady water flow equations. The equation system consists of the horizontal momentum equations, the continuity equation and the k–ε turbulence closure model. The modelled reach (length of about 1300 m, width of 45–150 m, and an average slope of 0·0021) was discretized into a finite-difference numerical grid composed of 11 029 grid cells, with 269 in the longitudinal and 41 in the transverse direction. The bottom topography was obtained by the initial topographic survey carried out during the summer of 2003. Field observations suggest that only relatively minor net changes in bed topography occurred after the flow events, suggesting that the fixed grid assumption is reasonable. However, the complex planimetric channel shape required the use of variable cell sizes (ranging between 0·5 m and 4 m). As detailed in Rinaldi *et al*. (2008a) no bedforms were expected to be found during the simulated flow events because the channel bed is mainly composed of gravel. Consequently, hydraulic roughness was modelled using the Colebrook–White formula to predict a depth-averaged Chézy coefficient C_{2D} ($m^{1/2}$ s^{-1}):

$$C_{2D} = 18 \log\left(\frac{12h}{k_s}\right) \quad (1)$$

where h (m) is the flow depth and k_s (m) is the Nikuradse roughness length. The modelled area was divided into five different roughness classes: channel bed zone, channel bar zone, vegetated bar zone, bank zone and bank-toe zone. For the non-vegetated zone, it was assumed that $k_s = 3\ D_{50}$, (where D_{50} is the median grain size) considering a variable distribution of sediment sizes based on a series of grain size analyses in the different portions of the channel, whereas for the vegetated zone an average value of k_s was calculated using measured plant height as the local Nikuradse roughness length.

Numerical simulations were performed for all the selected flow events (Mengoni, 2004; Mengoni and Mosselman, 2005), discretizing each flow event into time steps of 6 seconds. This high resolution time interval was selected as necessary and appropriate to reconstruct the temporal changes in near-bank shear stresses for each event. Due to the complex bed topography, the relationship between near-bank shear stress and flow discharges at the selected bank profile 22 (Figure 5) shows a trend in which maximum shear stress values correspond to

Table II. Parameters used for the bank erosion modelling (for full details see Rinaldi *et al*., 2008a): τ_c, critical shear stress; k_d, erodibility coefficient; n, porosity; k_{sat}, saturated hydraulic conductivity; c', effective cohesion; ϕ', effective friction angle; ϕ^b, matric suction angle; γ_d, dry unit weight; γ_{sat}, saturated unit weight; n/a, not applicable

Parameters	Sediment layers				
	Loose gravel and cobbles (1)	Gravel (2)	Silt, sand and clay (3)	Massive sandy silt (4)	Sandy silt (5)
τ_c (Pa)	8·22	8·10	0·85	n/a	n/a
k_d (m^3 Ns^{-1})	n/a	$6{\cdot}14 \times 10^{6}$	$7{\cdot}1 \times 10^{-6}$	n/a	n/a
n (%)	40	40	33	39	45
k_{sat} (m s^{-1})	$6{\cdot}0 \times 10^{-4}$	$1{\cdot}2 \times 10^{-4}$	$1{\cdot}4 \times 10^{-7}$	$3{\cdot}2 \times 10^{-6}$	$2{\cdot}3 \times 10^{-6}$
c' (kPa)	n/a	n/a	4·7	3·9	3·3
ϕ' (degrees)	n/a	n/a	32·5	35·9	37·6
ϕ^b (degrees)	n/a	n/a	15–32·5	15–35·9	15–37·6
γ_d (kN m^{-3})	n/a	n/a	14·9	16·4	14·6
γ_{sat} (kN m^{-3})	n/a	n/a	19·0	20·2	19·9

DOI: 10.1002/esp

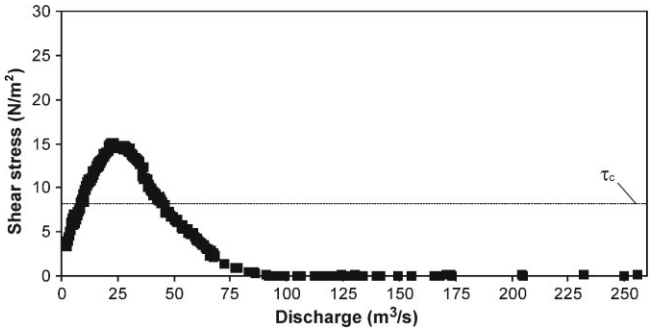

Figure 5. Results of hydrodynamic modelling: near-bank shear stress as a function of flow discharge at the bank profile 22 used for dynamic bank simulations: τ_c, critical shear stress for the basal gravel.

moderate flow discharges. This is because at lower discharges the main flow axis is concentrated along the low-water channel, directly in contact with the eroding outer bank, such that relatively high shear stresses are exerted at the bank toe. In contrast, at higher discharges the flow spreads across the point bar and lower shear stresses are simulated within the near-bank zone (Rinaldi *et al*., 2008a). This flow pattern has significant consequences for the temporal occurrence of fluvial erosion during the flow hydrograph, as discussed later.

The dynamic bank modelling involves the application of three submodels: (a) fluvial erosion; (b) groundwater flow; (c) bank stability. These submodels are linked using the computational sequence detailed in Darby *et al*. (2007). In each discrete time step this sequence consists of the following four-steps, the outputs of each step feeding into the inputs of the following one.

1. The hydrodynamic model discussed above is first used to evaluate the near-bank boundary shear stress (τ_b).
2. A fluvial erosion submodel (details below) is then applied to estimate the extent to which the bank profile is deformed by fluvial erosion. The bank profile morphology is then updated according to the simulated erosion.
3. A finite-element seepage analysis (details below) is then used to determine the spatial distribution of pore-water pressure within the simulated bank.
4. Finally, a limit equilibrium stability analysis (details below) is used to determine if the bank is liable to mass-failure under gravity. The bank profile morphology is then updated (for a second time in this sequence) in accordance with the simulated erosion.

This iterative cycle is then repeated, incrementing the time step, until the end of the simulation is reached. The black diamond symbols shown in the subplots in Figure 8 (below) indicate how each of the flow-event hydrographs investigated in this study was discretized into a series of time steps for these simulations.

Turning to the details of each of the bank process submodels, fluvial erosion was quantified using an excess shear stress formula (Partheniades, 1965; Arulanandan *et al*., 1980):

$$\varepsilon = k_d (\tau_b - \tau_c)^a \quad (2)$$

where ε (m s^{-1}) is the fluvial bank-erosion rate per unit time and unit bank area, τ_b (Pa) is the boundary shear stress applied by the flow, k_d (m^3 Ns^{-1}) and τ_c (Pa) are erodibility parameters (erodibility coefficient, k_d, and critical shear stress, τ_c) and a (dimensionless) is an empirically derived exponent, generally assumed to equal 1·0. Boundary shear stresses (τ_b) were obtained from the outputs of the hydrodynamic simulations, as discussed above, with τ_c and k_d parameterized as discussed in Rinaldi *et al*. (2008a) (see Table II). Figure 5 indicates that, based on these parameter values, flows causing erosion for the basal gravel range from about 8·5 m^3 s^{-1} to 45·9 m^3 s^{-1}, whereas higher discharges are not erosive. Having determined the parameter values used in equation (2), bank toe retreat was calculated by integrating Equation 2 across the given time interval of the time step (Δt) using:

$$FE = \varepsilon \Delta t = k_d (\tau_b - \tau_c)^a \Delta t \quad (3)$$

The finite-element seepage analysis was performed using the software SEEP/W (Geo-Slope International, 2001a) based on the following governing equation (Fredlund and Rahardjo, 1993):

$$\frac{\partial}{\partial x}\left(k_x \frac{\partial H}{\partial x}\right) + \frac{\partial}{\partial y}\left(k_y \frac{\partial H}{\partial y}\right) + Q = \frac{\partial \theta}{\partial t} \quad (4)$$

where H is the total head (m), k_x is the hydraulic conductivity in the x direction (m s^{-1}), k_y is the hydraulic conductivity in the y direction (m s^{-1}), Q is the unit flux passing in or out of an elementary cube (in this case an elementary square, given that the equation is in two-dimensions) (m^2 m^{-2} s^{-1}), θ is the volumetric water content (m^3 m^{-3}) and t is time (s). In our simulations, isotropic conditions were assumed for the hydraulic conductivity (i.e. $k_x = k_y$). To solve Equation 4, the bank geometry was discretized using a total of 8010 rectangular and triangular cells, and divided into regions composed of materials with different hydraulic and sedimentary properties, according to the bank stratigraphy. Hydraulic conductivity function (or k curve) and water content function (or characteristic curve) were defined for each layer based on grain sizes, measured values of porosity and saturated hydraulic conductivity, following the procedure described in Rinaldi *et al*. (2004) and Darby *et al*. (2007), and summarized here as follows. A range of empirical relations were initially defined for each type of material (Green and Corey, 1971; Van Genuchten, 1980; Fredlund *et al*., 1994) based on the grain size distribution, including curves already used in previous studies (Rinaldi *et al*., 2004; Darby *et al*., 2007) for bank sediments with similar characteristics. The resulting functions were constrained (by displacing the curves vertically) to fit measured values (see Table II) of porosity (n) and saturated hydraulic conductivity (k_{sat}). Porosity was obtained by laboratory analysis of single samples removed from each layer of sediment, whereas for the saturated hydraulic conductivity it was possible to perform Amoozemeter tests *in situ* (Amoozegar, 1989) only for the most superficial layers 4 and 5. For the remaining layers, saturated conductivity was initially assumed from values reported in the literature for similar material types. A further refinement of the curves (particularly for the layers lacking measurements) was undertaken via model calibration (i.e. by forcing best agreement between calculated and measured total head) simulations at the bank location where the two piezometers were installed, which is about 55 m upstream of the simulated bank (Luppi, 2004, 2007; Rinaldi *et al*., 2008a). Although variations in ground water level from the simulated bank profile to the location of the piezometers can be expected, we used the data at the two piezometers to constrain the conductivity and characteristic curves of the bank sediments, which are identical at the two locations.

Boundary conditions along the borders of the finite-element grid were defined as follows (Rinaldi *et al*., 2008a): (1) for the

DOI: 10.1002/esp

nodes along the bank profile, a total head versus time function was defined using the flow hydrograph; (2) for the nodes at the top of the bank, a rainfall intensity versus time function was assigned using the time-series rainfall data monitored at the gauging station 2 km upstream; (3) for the lower horizontal boundary and for the right vertical boundary, a zero flux boundary function was assigned, these regions being always saturated, whereas for the left vertical boundary, the infinite elements option was preferred to account for possible horizontal saturated and unsaturated fluxes. Finally, the initial conditions were defined using the same water table depth as that measured at the two piezometers installed in the bank before the start of each simulated event. Note that the groundwater flow modelling as undertaken herein is identical to previous studies on riverbank modelling (Dapporto *et al.*, 2001, 2003; Rinaldi *et al.*, 2004), but with the bank profile deformed to accord with the fluvial erosion simulated at the end of each discrete time step, as per the four-step computational sequence described previously.

The bank stability analysis was undertaken using the software SLOPE/W (Geo-Slope International, 2001b), which computes the factor of safety of the bank by applying limit equilibrium methods. This software is integrated with SEEP/W in such a way that the results (pore-water pressure distributions) of the groundwater flow model are used as input data for the stability analysis. Confining pressure is taken into account by specifying the water surface elevation. The Mohr–Coulomb failure criterion in terms of effective stress is used in the case of positive pore-water pressure, whereas the extended Fredlund *et al*. (1978) failure criterion for unsaturated soils is used in the case of negative pore-water pressure. For each time step, the factor of safety for shear-type cantilever failure is also computed, since this mechanism becomes important when the basal fluvial erosion is taken into account. Cantilever analysis is restricted to the shear-type failure (Thorne and Tovey, 1981), which is the most common type observed along the simulated bank, with the factor of safety expressed as:

$$F_s = \frac{\sum_i L_i C_{Ti}}{\sum \gamma_i A_i} \tag{5}$$

where L_i is the vertical length (layer i) of the cantilever block (m), C_{Ti} is the total cohesion (layer i) of the cantilever block (kPa), γ_i is the unit weight (layer i) of the cantilever block (kN m^{-3}), and A_i is the cross-sectional area (layer i) of the cantilever block (m^2).

Any model is an idealization of reality and so it is helpful to briefly summarize the main limitations of the bank stability analysis. First, confining forces due to the water in the river are not taken into account in the cantilever analysis; however, this simplification does not bias the results because the cantilever blocks in fact always develop above the river stage. Second, our simulations do not account for the potential deposition of basal gravel or failed material derived from mass failures of the cohesive layer, the latter being assumed to be completely and instantaneously removed by the flow. This is a reasonable assumption in the case of the Cecina River because of its relatively high energy; indeed our field observations reveal that only a very limited quantity of bank-derived fine sediments remain in storage at the bank toe after flow events. Finally, although recent work (Fox *et al.*, 2007; Wilson *et al.*, 2007) has started to explore the influence of seepage forces on bank stability, for reasons of simplicity we neglect these processes. As such, our analysis may potentially overestimate the stability of the modelled streambanks, although any error is likely to be small as field observations suggest that such processes are not significant at the study site.

Results and Discussion

Six numerical simulations were performed for a total of seven flow events observed during the monitoring period: (1) flow event 1 (1/11/2003–4/11/2003; Q_{peak} = 86·4 m^3 s^{-1}); (2) flow event 2 (24/11/2003–1/12/2003; Q_{peak} = 256·0 m^3 s^{-1}); (3) flow event 3 (29/12/2003–1/1/2004; Q_{peak} = 59·6 m^3 s^{-1}); (4) flow event 4 (17/1/2004–28/1/2004; Q_{peak} = 206·7 m^3 s^{-1}); (5) flow event 5 (18/2/2004–4/3/2004; Q_{peak} = 167·8 m^3 s^{-1}); (6) flow events 6 and 7 (17/4/2004–5/5/2004, Q_{peak} = 181·8 m^3 s^{-1}; and 5/5/2004–28/5/2004, Q_{peak} = 203·8 m^3 s^{-1}). The last simulation combines two events because the seventh event is a continuation of the sixth.

The initial bank geometry for each simulation was defined according to the latest available topographic measurements before the event. Comparisons between calculated and measured bank profiles for each simulated event are first visualized qualitatively in Figure 6 (Luppi, 2007), with a quantitative comparison between measured and predicted volumes of eroded sediment then provided in Figure 7. From the bank profiles plotted in Figure 6 it is evident that for event 1 the model correctly predicts that only bank-toe erosion occurs; this compares with the larger magnitude event 2 for which both processes (fluvial erosion and mass failure) are correctly predicted to occur, even if the bank-toe erosion is slightly overestimated (see below). For event 3, the model slightly underestimates the observed fluvial erosion, and does not predict mass failures, although in fact a minor failure did occur. The predictions for event 4 are particularly poor (see below) in that the observed fluvial erosion is clearly underestimated and the simulation fails to predict the mass failures that are observed in reality. In the case of events 5 and 6–7, both bank-toe erosion and mass failures are correctly predicted to occur.

We have assessed the extent to which the simulations match the observations by plotting simulated and observed eroded sediment volumes, discriminated by the eroding process, in Figure 7. Using the mean discrepancy ratio (*Me*) and correlation coefficient (r^2) as measures of fit (*Me* = r^2 = 1 for perfect fit), it is evident that the model predicts the fluvially eroded volumes of sediment well, with just a small underprediction on average (*Me* = 0·90, r^2 = 0·767). However, this is not surprising, as the erodibility parameter of the packed gravel was calibrated by forcing optimal agreement between the simulated and observed bank-toe position. In contrast, underprediction of the sediment volumes eroded by mass-wasting is significant (*Me* = 0·55, r^2 = 0·616), albeit primarily due to a failure to predict the mass-wasting events observed during events 3 and 4, as noted previously. Overall, agreement between the total volumes of eroded sediment estimated via model prediction and observation are acceptable (*Me* = 0·72, r^2 = 0·392). In any event, the results of the simulations remain valuable because they enable us to discriminate the contribution of each of the main bank erosion processes to the total eroded volume. Such information is extremely difficult to obtain by monitoring techniques, which are usually only able to provide data at a coarser timescale, at best perhaps resolving individual flow events. Therefore, the seven simulated events are used in this paper to investigate in detail the timing, rates and interaction among the different bank processes.

Time series of factor of safety, with respect to slide and cantilever failure mechanisms, and of volumes of eroded

DOI: 10.1002/esp

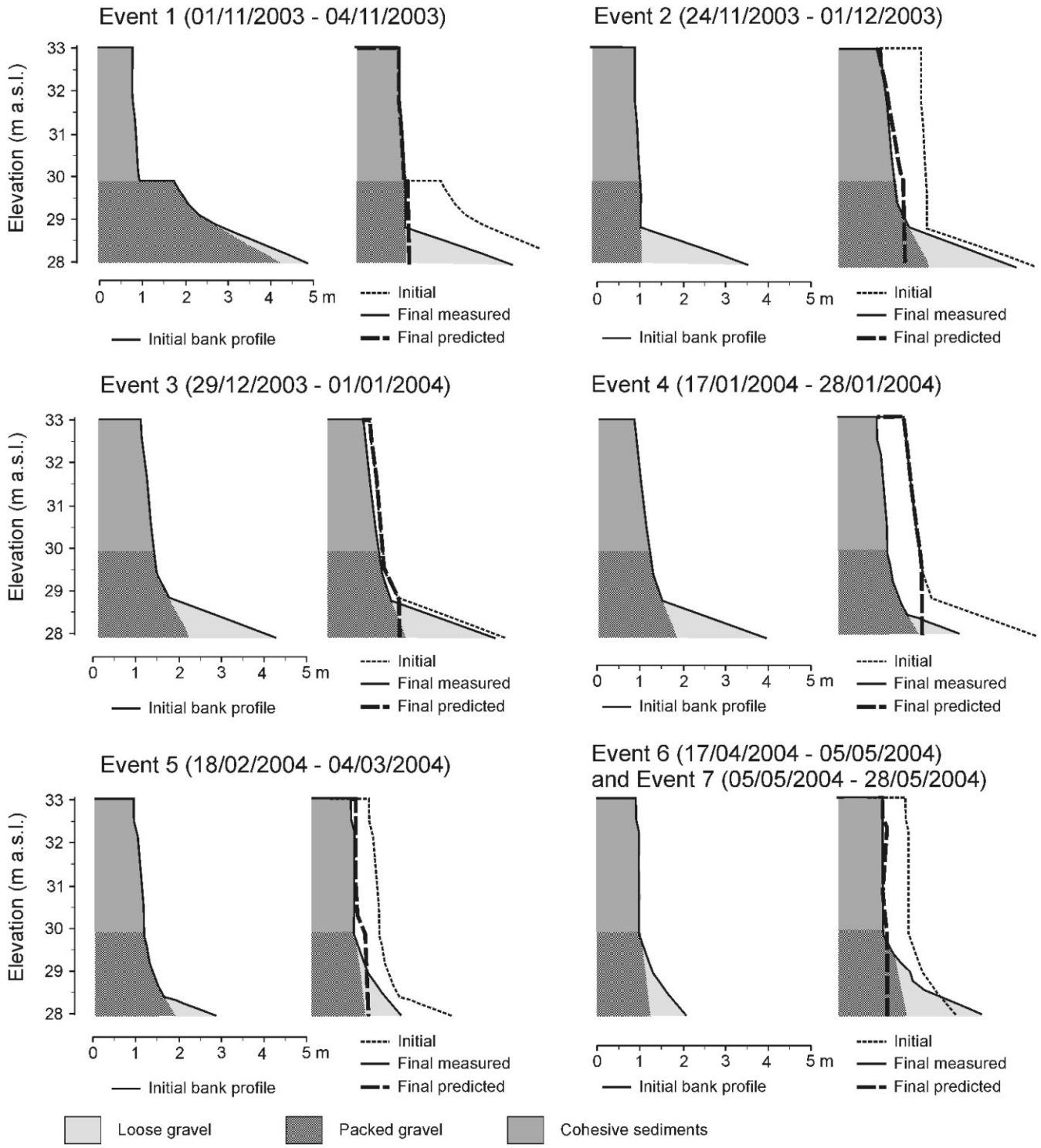

Figure 6. Measured and predicted bank changes at bank profile 22 for the simulated flow events. Prediction of basal bank profile is referred to the packed gravel.

sediment contributed by fluvial erosion and mass failures were produced for each of the seven simulated events (Figure 8), and a summary of the timing of onset, duration and volumes of eroded sediment for each erosive episode is provided in Table III. These results show that the occurrence of processes responsible for bank retreat (fluvial erosion, slide failure and cantilever failure) and their relative combinations differ for each event. As discussed below, this is due to variations in the following controlling factors: (1) initial bank conditions (geometry, water content); (2) flow event characteristics (rainfall, hydrograph). Since the initial (water content) conditions and flow event characteristics are in part related to seasonal hydrological conditions, it is possible to identify some seasonal controls on the simulated bank erosion processes. To discuss this aspect in more detail, it is useful to refer to Table IV, where the main hydrological characteristics of each event are summarized. Key results for each simulation are summarized as follows.

- *Flow event 1* (1/11/2003–4/11/2003; Q_{peak} = 86·4 m^3 s^{-1}). This event was a typical early autumnal single peak, flashy, hydrograph related to a short and relatively intense storm. Despite the relatively low peak discharge, shear stresses at the bank toe were high (for the reason explained previously), and were responsible for generating the highest volume of fluvial erosion (2·81 m^3/m).

DOI: 10.1002/esp

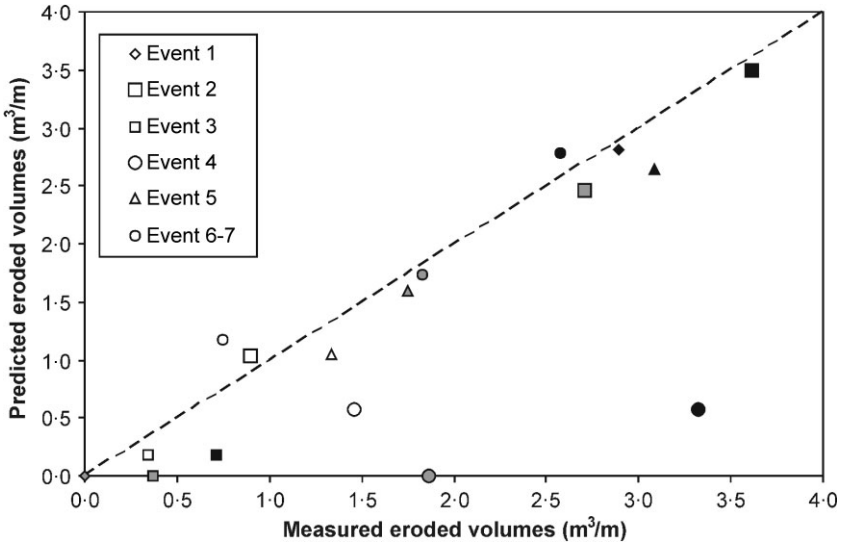

Figure 7. Comparison of predicted versus measured bank retreat showing the eroded volumes of bank sediment for each simulated flow event. The colour of the symbols indicates the erosion process: in white, fluvial erosion; in grey, mass failure; in black, the total volume. The dashed line is the line of perfect agreement.

Table III. Summary of the time of onset, duration, and volume of eroded sediment for the different processes. *N*, number of flow event (see Table I); *L*, total length of the flow event; T_0; time of onset of the process; *D*; duration of erosive episodes (indicated only for fluvial erosion, as for mass failures the process is considered instantaneous); *V*; volume of sediment delivered by each erosive process; V_{TOT}; total volume of eroded sediment for the event

		Fluvial erosion				Slide failure			Cantilever failure			
N	*L* (h)	T_0 (h)	*D* (h)	*V* (m³ m⁻¹)	V/V_{TOT} (%)	T_0 (h)	*V* (m³ m⁻¹)	V/V_{TOT} (%)	T_0 (h)	*V* (m³ m⁻¹)	V/V_{TOT} (%)	V_{TOT} (m³ m⁻¹)
1	120·8	5·75	5·25	1·13								2·81
		16·25	17·75	1·68	100							
2	199·5	7·50	8·00	0·08								
		57·25	19·75	0·44								
					30	82·50	2·09	70				3·51
						87·25	0·15					
						90·75	0·23					
		90·75	16·15	0·52								
3	45·0	3·50	10·75	0·18	100							0·18
4	78·7	15·00	14·00	0·57	100							0·57
5	328·5	56·25	23·00	0·12								
		95·75	115·75	0·59								
		219·75	108·75	0·34	40						60	2·64
									276·25	1·59		
6	609·2	2·75	203·75	0·34								
						183·25	1·11					
		210·5	34·75	0·05	38							
		250·00	359·25	0·65				40			22	2·78
									484·75	0·62		
7	460·8	0·00	26·00	0·01								
		37·00	42·50	0·02								
		83·75	377·00	0·11	100							0·14

However, this erosion did not trigger mass failures because: (a) the initial bank geometry, with a relatively low bank-toe slope angle, prevented the generation of cantilever blocks despite the high toe erosion (see Figure 6); and (b) peak river stage was relatively low and did not produce a sufficient increase in pore water pressures in the cohesive portion of the bank to trigger slide failures.

- *Flow event 2* (24/11/2003–1/12/2003; Q_{peak} = 256·0 m³ s⁻¹). This event represents a typical autumnal storm, with repeated and prolonged rainfall generating a long, multipeak, hydrograph, with the highest peak discharge of the monitoring period. Small amounts of fluvial erosion were predicted during the initial part of the event, with higher eroded volumes during the drawdown of the main peak, and during the final descending phase. However, although the total fluvial erosion (1·05 m³ m⁻¹) was lower than in the previous event, the conditions required to trigger mass failures (relatively high river stages and pore-water pressures) were nevertheless attained, in part due to the steep initial bank geometry inherited from the prior toe erosion. In fact, one major and two minor slides occurred during the latter phase of this event, contributing a sediment volume (2·47 m³ m⁻¹) that was the highest of the events simulated here.

DOI: 10.1002/esp

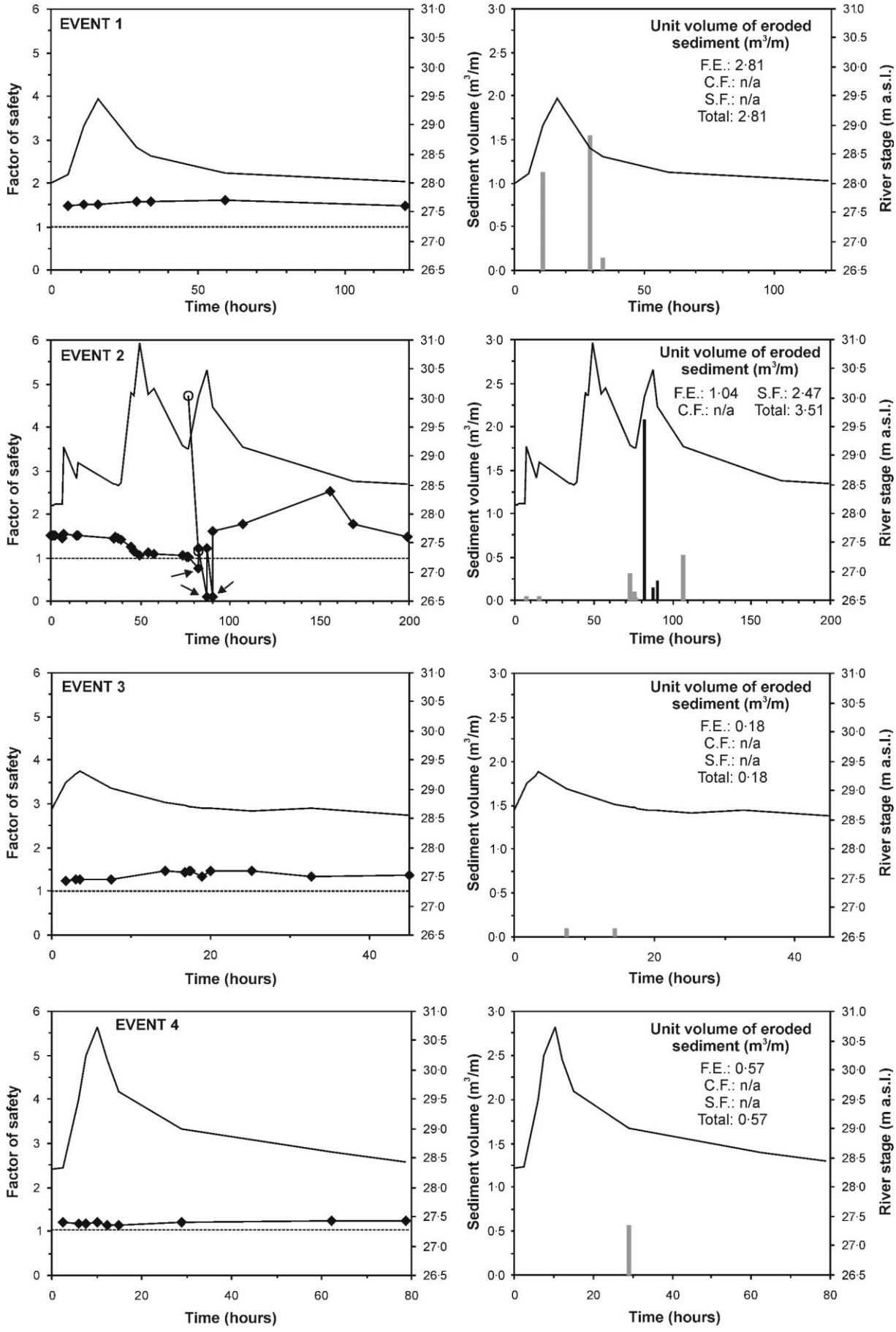

Figure 8. Results of bank dynamic modelling: trend of factor of safety for slide and cantilever failures (on the left), and eroded volumes of bank sediment (on the right) for the simulated flow events: F.E., fluvial erosion; S.F., slide failure; C.F., cantilever failure; n/a, not applicable. The event hydrograph is also shown (solid lines). The dotted horizontal lines indicate the critical factor of safety value of unity ($F_s < 1$ implies bank collapse), with the arrows indicating the onset of simulated failure episodes. Note that factor of safety data for the cantilever failures are plotted only for those points in time when a cantilevered (overhanging) bank profile is actually present.

DOI: 10.1002/esp

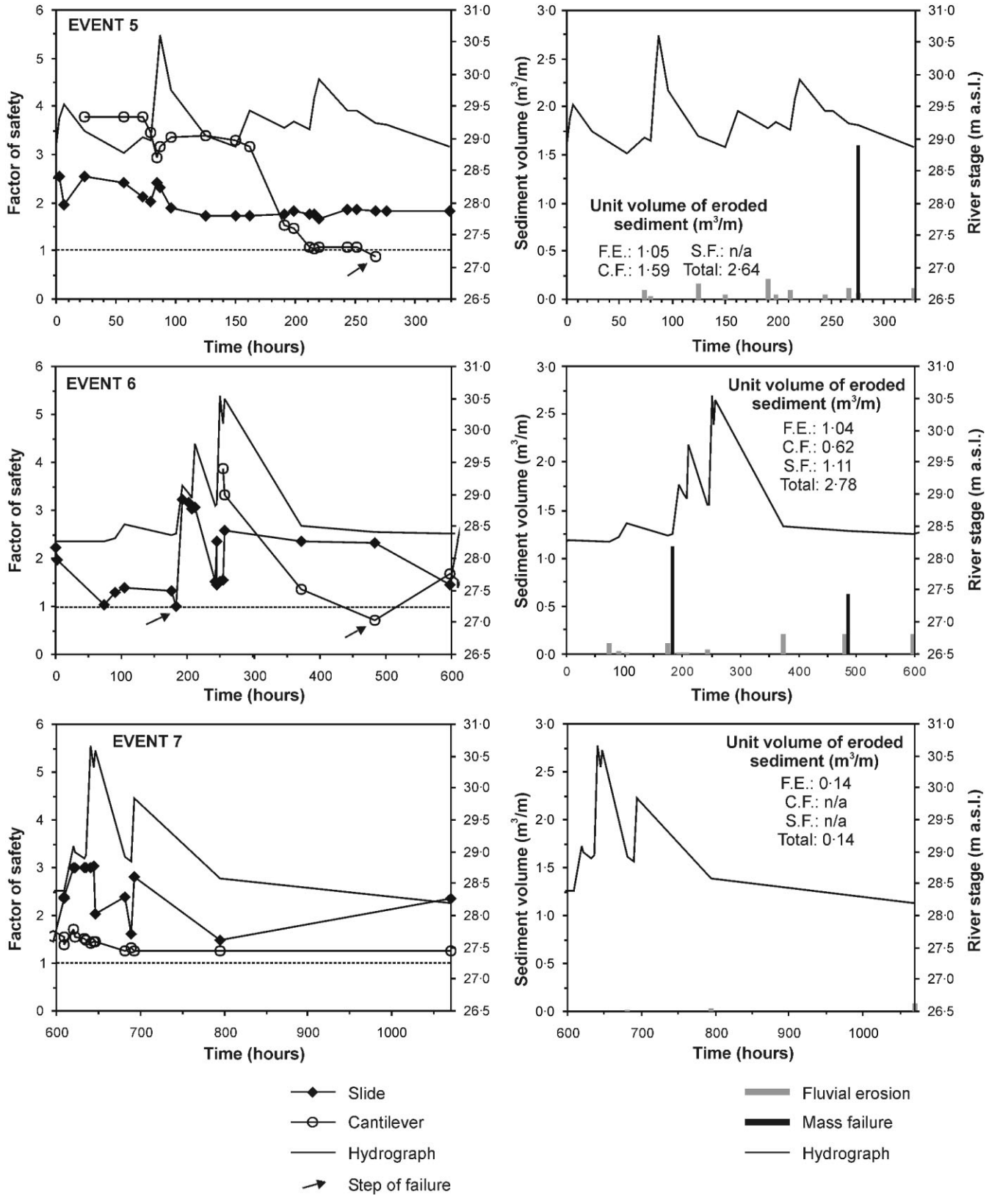

Figure 8. (*Continued*)

- *Flow event 3* (29/12/2003–1/1/2004; Q_{peak} = 59·6 m^3 s^{-1}). This event is similar to event 1 (single peak), but with a lower peak discharge and a very short length (45 hours). Because of the rapid rise and fall of the flow, relatively high shear stresses at the bank toe occurred only for a short time, so that the simulated bank toe erosion is very limited (0·18 m^3 m^{-1}). The relatively low rainfall and low peak river stage do not produce high pore-water pressures in the cohesive upper bank, which together with the small amount of simulated fluvial erosion therefore fails to trigger any mass failure episode.
- *Flow event 4* (17/1/2004–28/1/2004; Q_{peak} = 206·7 m^3 s^{-1}). This is another single peak, flashy, hydrograph, with the second highest peak river stage of the monitoring period (30·74 m a.s.l.), although rainfall at the monitored bank and recorded at the Ponte di Monterufoli was relatively

DOI: 10.1002/esp

Table IV. Summary of hydrological characteristics of the simulated flow events: *N*, number of simulated flow event; *L*, total length of the flow event; *R*, rainfall (recorded at the Ponte di Monterufoli gauging station); Q_{peak}, peak discharge; *H*, peak river stage (at the monitoring section); GWL_0, initial ground water level; GWL_m, maximum ground water level

N	Month	*L* (h)	Shape	*R* (mm)	Q_{peak} ($m^3\ s^{-1}$)	*H* (m a.s.l.)	GWL_0 (m a.s.l.)	GWL_m (m a.s.l.)
1	Early November	120·8	Single peak	29·8	86·4	29·60	28·15	29·20
2	Late November	199·5	Single peak	80·2	256·0	30·96	28·15	30·25
3	Late December	45·0	Single peak	13·2	59·6	29·32	28·29	29·30
4	Late January	78·7	Single peak	26·7	206·7	30·74	28·23	30·50
5	February	328·5	Multipeak	74·2	167·8	30·45	28·75	30·53
6	April	609·2	Multipeak	85·1	181·8	30·52	28·27	29·10
7	May	460·8	Multipeak	45·3	203·8	30·63	28·48	29·80

low (26·7 mm), while higher precipitation occurred in the upper portion of the catchment. For similar reasons to the previous event, the very rapid ascending phase was not able to produce any bank-toe retreat. Although a moderate amount of toe erosion (0·57 $m^3\ m^{-1}$) occurred during the slower falling limb of the hydrograph, this was not sufficient to generate a cantilever block. As previously noted, the mean bank retreat of this event was relatively low, but a local retreat of 0·63 m occurred at the selected bank profile 22. As a result of the short duration of the event and the relatively low rainfall at the bank, simulated pore-water pressures were not sufficiently high to trigger a mass failure and the model therefore underestimates bank-top retreat for this event, although the simulated factor of safety for slide failures (1·13) is close to 1 immediately after the peak stage.

- *Flow event 5* (18/2/2004–4/3/2004; Q_{peak} = 167·8 $m^3\ s^{-1}$). This event shares some of the characteristics of event 2, with a prolonged and multipeak hydrograph, but with lower total rainfall. Fluvial erosion was predicted intermittently throughout the flow hydrograph, providing a preparatory role for mass failure; in fact a cantilever failure (1·59 $m^3\ m^{-1}$) occurred during the late part of the hydrograph.
- *Flow event 6* (17/4/2004–5/5/2004, Q_{peak} = 181·8 $m^3\ s^{-1}$). Flow event 6, and the following event 7, are characterized here as two spring hydrographs. The simulation reproduces a very long, complex, and multipeak hydrograph event generated by a succession of rainfall episodes. Fluvial erosion was predicted to occur during various phases, while a slide failure (1·11 m^3/m) was predicted in an early stage of the hydrograph, at the beginning of the rising part of the first peak, as distinct from the other simulated events when mass failures were typically timed in the later phases of the events. The early onset of mass-wasting in this simulation was caused mainly by: (a) the pore-water pressures being relatively high at the beginning of the event, due to the particularly rainy antecedent period; and (b) the initial bank geometry being unfavourable due to the antecedent erosion. Finally, a cantilever failure (0·62 $m^3\ m^{-1}$) occurred during the drawdown of the main peak.
- *Flow event 7* (5/5/2004–28/5/2004, Q_{peak} = 203·8 $m^3\ s^{-1}$). This event is essentially a continuation of the previous one but a new peak, characterized by a rapid rising phase followed by a secondary one, was observed. During this event fluvial erosion was the only predicted process, occurring during various phases of the hydrograph but with only very small amounts (0·14 $m^3\ m^{-1}$).

Figure 9 summarizes the occurrence of processes and associated volumes of sediment delivered to the channel for each of the simulated flow events. It is evident that in early autumnal flashy events, mainly characterized by single peak hydrographs, fluvial erosion is the dominant process. Events occurring during November and some winter events tend to be prolonged and multipeaked and as such are generally dominated by mass failures (Lawler, 1992; Rinaldi *et al.*, 2004). Spring events are characterized by intermediate conditions, so that a combination of all the different processes (fluvial erosion, slide, cantilever) is evident. In terms of the volumes of sediment eroded by each process, fluvial erosion accounted for 6·83 $m^3\ m^{-1}$ from a total volume of 12·63 $m^3\ m^{-1}$ (54%) eroded across all seven events, while mass failures produced 5·79 $m^3\ m^{-1}$ (46%), of which 2·21 $m^3\ m^{-1}$ was from cantilevers and 3·58 $m^3\ m^{-1}$ was from slide failures. This reinforces the point that fluvial erosion and mass failures are both significant contributors to the total volume of the eroded sediment.

To analyse the variability in the relative timing of the different processes within the flow-event hydrographs, the timing of onset (T_0) of each process was first normalized in

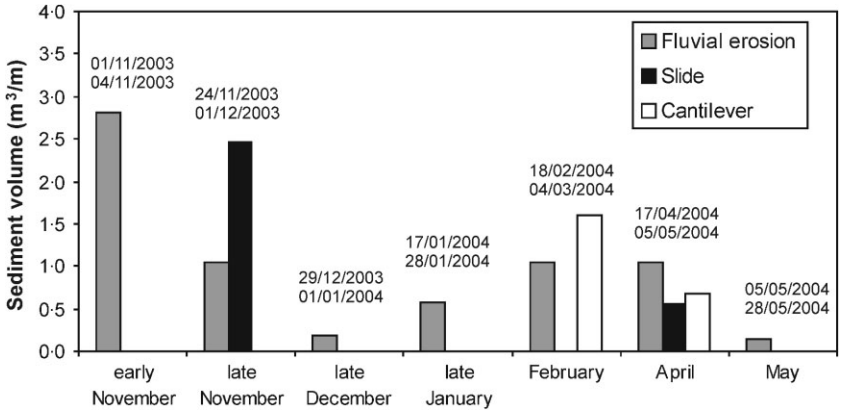

Figure 9. Distribution of processes and summary of eroded volumes of bank sediment during the simulated flow events.

DOI: 10.1002/esp

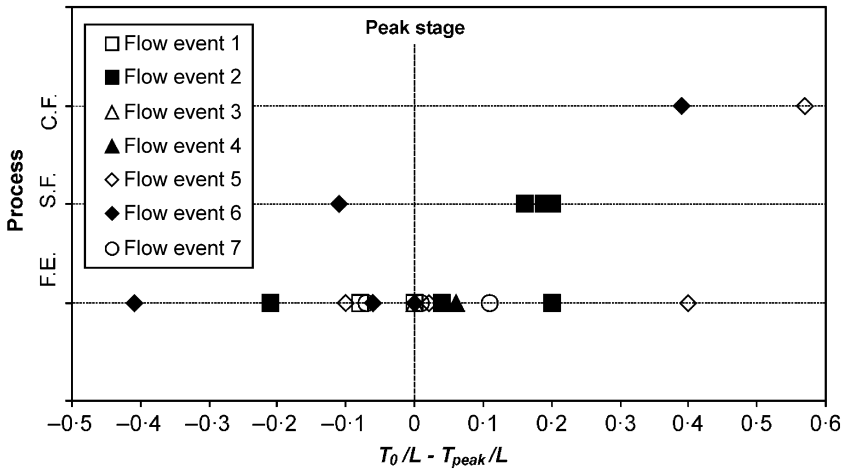

Figure 10. Timing of the onset of the different processes within the flow hydrograph: T_0, time of onset; L, length of the hydrograph; T_0/L; non-dimensionalized time of onset; T_{peak}/L, non-dimensionalized time of peak discharge; F.E., fluvial erosion; S.F., slide failure; C.F., cantilever failure.

relation to the total duration of the event (L). By defining the timing of the main peak in the same way (i.e. T_{peak}/L) we constructed a non-dimensional parameter ($T_0/L - T_{peak}/L$) for which values of zero correspond to the peak stage of each event, negative values correspond to the pre-peak phase and positive values correspond to the post-peak phase. Using this measure, the occurrence of each of the three erosion processes (fluvial erosion, slide, cantilever) within the simulated flow events is assessed in Figure 10. From this graph it is evident that:

1. Fluvial erosion is distributed throughout the duration of the flow hydrographs analysed here, but tends to occur in close proximity to the peak phase only for the relatively minor flow events, whereas for the larger flows fluvial erosion tends to occur during the ascending or descending phases of the hydrograph. This is due to the specific relationship between near-bank shear stress and flow discharge (Figure 5), such that for $Q > 46{\cdot}2$ m^3 s^{-1} near-bank shear stresses are not erosive. As discussed previously this effect is due to the steering of the high-velocity core away from the outer bank during high flows.
2. Slide failures generally occur during the early post-peak phase of the hydrograph (event 2), or even in the ascending phase (event 6), as they are triggered by elevated pore-water pressures and relatively lower hydrostatic confining river pressures. In event 6, failure occurs during the rising phase because the unfavourable pore-water pressures are sufficient to trigger the failure, and because the confining pressures on the cohesive portion of the bank remain very limited.
3. Cantilever failures occur during the later phases of the flow hydrograph, as they are triggered by the cumulative effects of fluvial erosion at the bank toe.

For the case of mass failures the above findings contrast with those from a previous study (Rinaldi *et al.*, 2004) on a similar riverbank on the Sieve River in central Italy. On the Sieve River, bank-failure episodes were always timed after the peak flow stage, during the drawdown phase of the hydrograph. This difference can be explained by the fact that the Sieve River simulations were performed for a constant bank geometry (i.e. excluding bank-toe deformation by fluvial erosion). More recent, fully integrated simulations at the Sieve study site (Darby *et al.*, 2007), which include the deforming effects of fluvial erosion, predict the onset of mass failures in other phases of the hydrograph, consistent with our results from the Cecina River. This suggests that previous studies (Twidale, 1964; Thorne, 1982; Springler *et al.*, 1985; Lawler *et al.*, 1997; Rinaldi *et al.*, 2004), which tend to emphasize the occurrence of mass-failures in the drawdown phase of the flow hydrograph, but which have neglected the interactions between fluvial erosion and mass-wasting, may provide a misleading picture of the true timing of mass-failure events, at least for banks types (i.e. with a cohesive upper portion overlying a gravel toe), river characteristics (gravel-bed rivers with relatively high energy) and hydrological conditions (high variability in flow discharges) common in the study area.

We have synthesized our simulation results into a conceptual model of bank response to hydrographs with varying shapes and peak discharges (Figure 11). The hydrograph in Figure 11A is characterized by a lower peak discharge, but has a longer duration of erosive flows covering the range between the discharges associated with the onset (Q_{OFE}) and cessation (Q_{CFE}) of fluvial erosion. Under these conditions, fluvial erosion is the dominant process. Slide failures are unlikely to occur, because insufficient positive pore-water pressures are developed, but cantilever failures triggered by basal toe erosion are possible in the latter part of the event, depending on the initial bank geometry and the amount of basal erosion. In contrast, the hydrograph in Figure 11B represents an example of an intense, flashy, flood with a much higher peak discharge, but very steep ascending and descending phases, so that (hydraulically) erosive flows are experienced for a shorter duration. For these hydrographs, fluvial erosion is less effective than in the previous case, whereas slide failures are more likely to occur around the peak phase (primarily during the descending phase but in some cases even before the peak). The final phase of fluvial erosion may be effective in remodelling the bank toe (e.g. by removing failed material) and possibly triggering cantilever failures during the final phases of the hydrograph.

A final point of discussion here regards the possible relationship between bank erosion processes and flow intensity. In this respect, a basic question is whether or not fluvial erosion and/or mass failures increase in occurrence and magnitude with increasing flow discharge. As previously discussed, earlier studies (e.g. Hooke, 1980) have found poor correlations between peak flow discharge and bank erosion rate. Similarly, our results (Figure 4B) also indicate a high degree of variability in the relationship between bank retreat and peak flow discharge. However, our simulations have the advantage that they enable us to discriminate the relative contributions of fluvial

DOI: 10.1002/esp

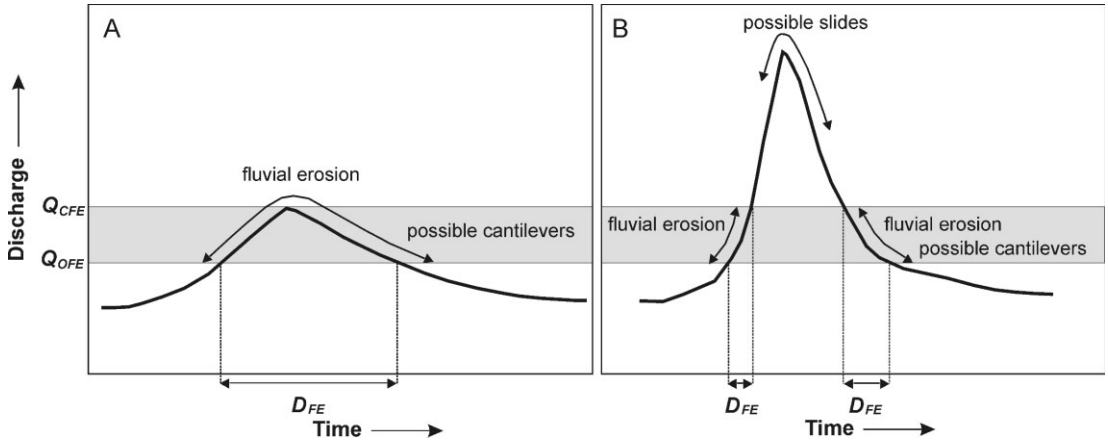

Figure 11. Schematic conceptual model of bank responses to hydrographs with different shapes and peak stages. (A) Hydrograph with lower peak discharge and relatively slow ascending and descending phases. (B) Hydrograph with higher peak discharge and relatively fast ascending and descending phases. Q_{OFE}, discharge of onset for fluvial erosion; Q_{CFE}, discharge of cessation for fluvial erosion; D_{FE}, duration of fluvial erosion.

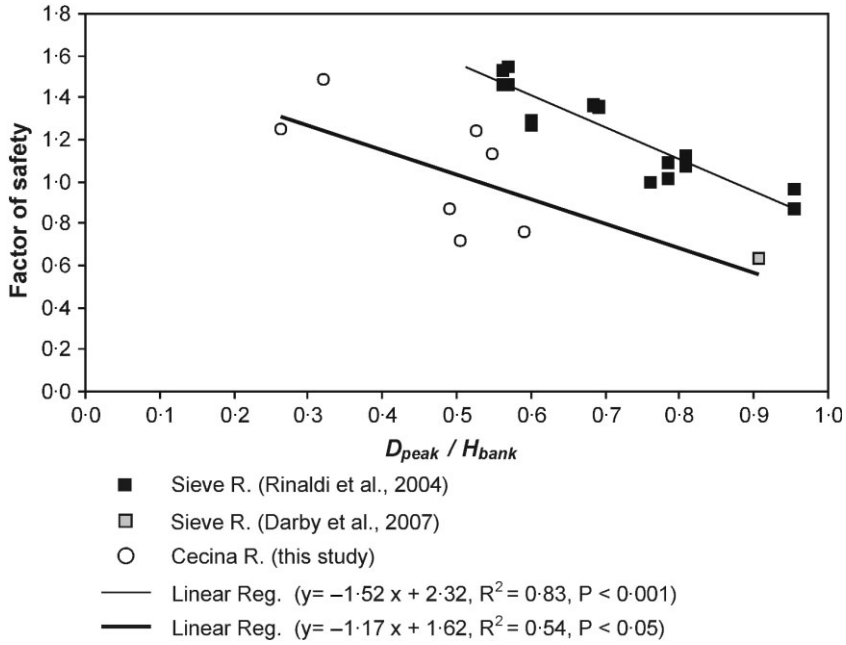

Figure 12. Minimum factor of safety for slide failures as a function of non-dimensionalized peak flow depth: comparison of results from this study with results of previous bank simulations. D_{peak}: peak flow depth; H_{bank}: bank height; D_{peak}/H_{bank}: nondimensionalized peak flow depth.

erosion and mass failure to bank retreat and thus identify the relationships between peak flow conditions and the intensity of specific erosion processes. Moreover, we can also include data derived from similar bank erosion modelling investigations carried out on the Sieve River (Rinaldi *et al.*, 2004; Darby *et al.*, 2007), recalling that the study by Rinaldi *et al.* (2004) considered only mass failures of the upper cohesive portion of the bank whereas the study by Darby *et al.* (2007) included bank deformation by fluvial erosion and mass-wasting, as for the Cecina River simulations carried out in this study.

Considering the relationship between mass failure and flow intensity, Figure 12 plots the minimum factor of safety in relation to the peak flow discharge. To make the data from the Sieve and Cecina studies comparable, we have normalized the peak flow depth (D_{peak}) in relation to the total height of the bank (H_{bank}). The study by Rinaldi *et al.* (2004) excluded fluvial erosion and considered bank stability with respect only to slide failures, while the other simulations include bank deformation by fluvial erosion, as well as considering both slide and cantilever failure processes. If all the data are considered ($n = 25$), they are clearly scattered, with a low R^2 value of 0·36. In contrast, if the data are separated into two series comprising (i) simulations with no fluvial erosion (Rinaldi *et al.*, 2004), and (ii) dynamic simulations including both fluvial erosion and mass wasting (Darby *et al.*, 2007; this study), significant regressions are obtained ($R^2 = 0{\cdot}83$, $n = 17$, $P < 0{\cdot}001$ for the first regression, and $R^2 = 0{\cdot}54$, $n = 8$, $P < 0{\cdot}05$ for the second), although the second relationship is clearly weaker than the first. Nevertheless, in both cases there is a clear decrease in the simulated factor of safety with increasing peak river stages, while the offset between the two relationships also highlights the significant destabilizing role of fluvial erosion, with factors of safety for the second series (with fluvial erosion) typically 50% lower than for the first. In summary, the evident decrease of factor of safety with increasing peak flow is clearly related to the fact that higher river stages tend to produce more unfavourable pore-water pressure conditions, as already noted by Rinaldi *et al.* (2004), while the present study additionally highlights the need for the factor of safety to account correctly for fluvial erosion in order to avoid significant overpredictions of the factor of safety.

DOI: 10.1002/esp

Conclusions

In this paper we conducted a series of numerical simulations characterizing bank retreat for a riverbank of the Cecina River. The modelling involved linking different hydraulic and geotechnical submodels at each of a series of discrete time steps throughout a range of flow-event hydrographs. Seven significant flow events, monitored during the period 2003–2004, and representative of the typical range of annual hydrographs, were simulated. Results of the simulations show that the occurrence of bank erosion processes (fluvial erosion, slide failure, cantilever failure) and their respective combinations differ significantly between each event. These variations are induced by variations in the initial bank conditions and hydrograph characteristics, which in turn are related mainly to seasonal hydrological characteristics. Early autumnal flashy events are mainly characterized by single peak hydrographs, with fluvial erosion the dominant process. Events occurring during November and some other winter events are generally more prolonged and multipeaked, tending to be dominated by mass failures. Spring events are characterized by intermediate conditions, so that a combination of all the different bank erosion processes occur, at least in the case of the particularly rainy springs that characterized our study period.

We have synthesized our findings in the form of a conceptual model of bank response to hydrographs of different shape and intensity. In this model the duration of moderate erosive flows determines the occurrence and quantity of fluvial erosion, rather than the peak discharge. In contrast, slide failures, being influenced strongly by pore-water pressure conditions, are controlled primarily by higher river stages and in fact tend to occur during the peak phases of the hydrograph. In contrast, cantilever failures more typically occur within the later phases of the hydrograph, being induced by the cumulative effects of fluvial erosion.

In closing it must be noted that our results are limited to the specific conditions encountered at the Cecina study site, and the limited number of simulations makes it difficult to generalize these findings to other situations. However, our conceptual model appears to be more generally applicable to channel bends, where moderate flows have a direct impact on the outer eroding bank, whereas for higher discharges a diversion of flow across a chute-channel occurs, causing a drastic reduction of shear stresses along the eroding bank.

Acknowledgements—This research was supported by the Royal Society (Joint Project Grant 15077), by the project 'Monitoraggio e modellazione dei processi di erosione di sponde fluviali' (2002/04) (Fondo Ateneo ex 60% – Università di Firenze), and by the programme MIUR (Ministero Italiano dell'Istruzione, Università e Ricerca) 'Incentivazione alla mobilità di studiosi stranieri e italiani residenti all'estero' (L. B. Teruggi). The following persons are acknowledged for their support at different stages of the research: S. Dapporto, F. Vannacci, F. Canovaro, F. Agresti, L. Coppi and S. Attardo. Furthermore, F. Mansella, E. Di Carlo and B. Mazzanti of the National Hydrographic Survey of Pisa and Florence are acknowledged for providing hydrological data. We are also grateful to the two anonymous referees for their constructive reviews on the first draft of this paper.

References

Abernethy B, Rutherfurd ID. 1998. Where along a river's length will vegetation most effectively stabilise stream banks? *Geomorphology* **23**: 55–75.

Abernethy B, Rutherfurd ID. 2000. The effect of riparian tree roots on the mass-stability of riverbanks. *Earth Surface Processes and Landforms* **25**: 921–937.

Amoozegar A. 1989. A compact constant-head permeameter for measuring saturated hydraulic conductivity of the vadose zone. *Journal of the Soil Science Society of America* **53**: 1356–1361.

Arulanandan K, Gillogley E, Tully R. 1980. *Development of a Quantitative Method to Predict Critical Shear Stress and Rate of Erosion of Natural Undisturbed Cohesive Soils*. Report GL-80-5, U.S.Army Engineers, Waterways Experiment Station: Vicksburg, Mississippi.

Casagli N, Rinaldi M, Gargini A, Curini A. 1999. Monitoring of pore water pressure and stability of streambanks: results from an experimental site on the Sieve River, Italy. *Earth Surface Processes and Landforms* **24**: 1095–1114.

Couper PR, Maddock IP. 2001. Subaerial river bank erosion processes and their interaction with other bank erosion mechanisms on the River Arrow, Warwickshire, UK. *Earth Surface Processes and Landforms* **26**: 631–646.

Dapporto S, Rinaldi M, Casagli N. 2001. Mechanisms of failure and pore water pressure conditions: analysis of a riverbank along the Arno River (Central Italy). *Engineering Geology* **61**: 221–242.

Dapporto S, Rinaldi M, Casagli N, Vannocci P. 2003. Mechanisms of riverbank failure along the Arno River, Central Italy. *Earth Surface Processes and Landforms* **28**(12): 1303–1323.

Darby SE, Rinaldi M, Dapporto S. 2007. Coupled simulations for fluvial erosion and mass wasting for cohesive river banks. *Journal of Geophysical Research* **112**: F03022. DOI: 10.1029/2006JF000722

Fox GA, Wilson GV, Periketi R, Cullum FF. 2006. Sediment transport model for seepage erosion of streambank sediment. *Journal of Hydrologic Engineering* **11**(6): 603–611.

Fox GA, Wilson GV, Simon A, Langendoen E, Akay O, Fuchs JW. 2007. Measuring streambank erosion due to ground water seepage: correlation to bank pore water pressure, precipitation, and stream stage. *Earth Surface Processes Landforms* **32**(10): 1558–1573.

Fredlund DG, Rahardjo H. 1993. *Soil Mechanics for Unsaturated Soils*. Wiley: New York.

Fredlund DG, Morgenstern NR, Widger RA. 1978. The shear strength of unsaturated soils. *Canadian Geotechnical Journal* **15**(3): 312–321.

Fredlund DG, Xing A, Huang S. 1994. Predicting the permeability function for unsaturated soils using the soil-water characteristic curve. *Canadian Geotechnical Journal* **31**: 533–546.

Geo-Slope International. 2001a. *SEEP/W for Finite Element Seepage Analysis, Version 5, User Manual*. Calgary, Alberta.

Geo-Slope International. 2001b. *SLOPE/W for Slope Stability Analysis, Version 5, User Manual*. Calgary, Alberta.

Green RE, Corey JC. 1971. Calculation of hydraulic conductivity: a further evaluation of some predictive methods. *Proceedings of the Soil Science Society of America* **35**: 3–8.

Hooke JM. 1980. Magnitude and distribution of rates of river bank erosion. *Earth Surface Processes and Landforms* **5**: 143–157.

Julian JP, Torres R. 2006. Hydraulic erosion of cohesive riverbanks. *Geomorphology* **76**: 193–206.

Kean JW, Smith JD. 2006a. Form drag in rivers due to small-scale natural topographic features: 1. Regular sequences. *Journal of Geophysical Research* **111**: F04009. DOI: 10.1029/2006JF000467

Kean JW, Smith JD. 2006b. Form drag in rivers due to small-scale natural topographic features: 2. Irregular sequences. *Journal of Geophysical Research* **111**: F04010. DOI: 10.1029/2006JF000490

Lawler DM. 1992. Process dominance in bank erosion systems. In *Lowland Floodplain Rivers: Geomorphological Perspectives*, Carling PA, Petts GE (eds). Wiley: Chichester; 117–143.

Lawler DM. 1993. The measurement of river bank erosion and lateral channel change. *Earth Surface Processes and Landforms* **18**: 777–821.

Lawler DM. 2005a. Defining the moment of erosion: the principle of thermal consonance timing. *Earth Surface Processes and Landforms* **30**(13): 1597–1615.

Lawler DM. 2005b. The importance of high-resolution monitoring in erosion and deposition dynamics studies: examples from estuarine and fluvial systems. *Geomorphology* **64**: 1–23.

Lawler DM, Thorne CR, Hooke JM. 1997. Bank erosion and instability. In *Applied Fluvial Geomorphology for River Engineering and Management*, Thorne CR, Hey RD, Newson MD (eds). Wiley: Chichester; 137–172.

Luppi L. 2004. *Monitoraggio e modellazione del rapporto fiume-falda*

ed effetti sulla stabilità di una sponda del Fiume Cecina. MS thesis, University of Firenze, Firenze; 167 pp.

Luppi L. 2007. *Studio dei processi di erosione di sponde fluviali e influenza della vegetazione riparia sulla stabilità*. PhD Thesis, University of Firenze, Firenze.

Mengoni B. 2004. *River width adjustments: large-scale and local-scale approaches*, PhD Thesis, University of Florence, Italy.

Mengoni B, Mosselman E. 2005. Analysis of river bank erosion processes: Cecina river, Italy. *Proceedings RCEM: River, Coastal and Estuarine Morphodynamic*, 4–7 October, Urbana Champaign, Illinois; 943–951.

Papanicolaou AN, Elhakeem M, Hilldale R. 2007. Secondary current effects on cohesive river bank erosion. *Water Resources Research* **43**: W12418. DOI: 10.1029/2006WR005763

Partheniades E. 1965. Erosion and deposition of cohesive soils. *Journal of the Hydraulics Division, American Society Civil Engineers* **91**: 105–139.

Pollen NL. 2006. Temporal and spatial variability of root reinforcement of streambanks: Accounting for soil shear strength and moisture. *Catena* **69**. DOI: 10.1016/j.catena.2006.05.004

Pollen NL, Simon A. 2005. Estimating the mechanical effects of riparian vegetation on streambank stability using a fiber bundle model. *Water Resources Research* **41**: W07025. DOI: 10.1029/2004WR003801

Pollen-Bankhead N, Simon A. 2008. Enhanced application of root-reinforcement algorithms for bank-stability modelling. *Earth Surface Processes and Landforms*. DOI: 10.1002/esp.1690

Prosser IP, Hughes AO, Rutherfurd ID. 2000. Bank erosion of an incised upland channel by subaerial processes: Tasmania, Australia. *Earth Surface Processes and Landforms* **25**: 1085–1101.

Rinaldi M. 2003. Recent channel adjustments in alluvial rivers of Tuscany, Central Italy. *Earth Surface Processes and Landforms* **28**(6): 587–608.

Rinaldi M, Casagli N. 1999. Stability of streambanks formed in partially saturated soils and effects of negative pore water pressures: the Sieve River (Italy). *Geomorphology* **26**: 253–277.

Rinaldi M, Darby SE. 2008. Modelling river-bank-erosion processes and mass failure mechanisms: progress towards fully coupled simulations. In: *Gravel-Bed Rivers 6 – From Process Understanding to River Restoration*, Habersack H, Piegay H, Rinaldi M (eds). Series Developments in Earth Surface Processes, Vol. 11, Elsevier: Amsterdam; 213–239.

Rinaldi M, Casagli N, Dapporto S, Gargini A. 2004. Monitoring and modelling of pore water pressure changes and riverbank stability during flow events. *Earth Surface Processes and Landforms* **29**(2): 237–254.

Rinaldi M, Luppi L, Mengoni B, Darby SE, Mosselman E. 2008a. Numerical simulation of hydrodynamics and bank erosion in a river bend. *Water Resources Research* **44**. DOI: 10.1029/2008WR007008

Rinaldi M, Teruggi LB, Simoncini C, Nardi L 2008b. Dinamica recente ed attuale di alvei fluviali: alcuni casi di studio appenninici (Italia Centro-Settentrionale). *Il Quaternario* **21**(1B): 291–302.

Simon A, Collison AJ. 2002. Quantifying the mechanical and hydrological effects of vegetation on streambank stability. *Earth Surface Processes and Landforms* **27**: 527–546.

Simon A, Curini A, Darby SE, Langendoen EJ. 2000. Bank and near-bank processes in an incised channel. *Geomorphology* **35**: 193–217.

Simon A, Langendoen EJ, Collison A, Layzell A. 2003. Incorporating bank-toe erosion by hydraulic shear into a bank-stability model: Missouri River, Eastern Montana. In *World Water and Environmental Resources Congress and Related Symposia*, Bizier P, De Barry P (eds). American Society of Civil Engineers, Philadelphia, Pennsylvania. [CD ROM]

Simon A, Pollen NL, Langendoen EJ. 2006. Influence of two woody riparian species on critical conditions for streambank stability: Upper Truckee River, California. *Journal of the American Water Resources Association* **41**: 99–113.

Springer FM Jr, Ullrich CR, Hagerty DJ. 1985. Streambank stability. *Journal of Geotechnical Engineering* **111**(5): 624–640.

Thorne CR. 1982. Processes and mechanisms of river bank erosion. In *Gravel-bed Rivers*, Hey RD, Bathurst JC, Thorne CR (eds). Wiley: Chichester; 227–271.

Thorne CR, Tovey NK. 1981. Stability of composite river banks. *Earth Surface Processes and Landforms* **6**: 469–484.

Twidale CR. 1964. Erosion of an alluvial bank at Birdwood, South Australia. *Zeitschrift für Geomorphologie* **8**: 189–211.

Van De Wiel MJ, Darby SE. 2007. A new model to analyse the impact of woody riparian vegetation on the geotechnical stability of riverbanks. *Earth Surface Processes and Landforms* **32**(14): 2185–2198.

Van Genuchten MT. 1980. A closed-form equation for predicting the hydraulic conductivity of unsaturated soils. *Journal of the Soil Science Society of America* **44**: 892–898.

Wilson GV, Periketi RK, Fox GA, Dabney SM, Shields FD, Cullum RF. 2007. Seepage erosion properties contributing to streambank failure. *Earth Surface Processes and Landforms* **32**(3): 447–459.

WL Delft Hydraulics. 2006. *Delft3D-FLOW: Simulation of Multi-dimensional Hydrodynamic Flows and Transport Phenomena, including Sediments, User Manual*. WL Delft Hydraulics: Delft.